Quartz grain microtextures illuminate Pliocene periglacial sand fluxes on the Antarctic continental margin

Sandra Passchier[1], Melissa A. Hansen[1], Jessica Rosenberg[1,2]

[1]*Montclair State University, Department of Earth and Environmental Studies, 1 Normal Ave, Montclair NJ 07043, United States*

[2]*Present address: GEI consultants, 3065 Akers Mill Rd, Ste 235, Atlanta, GA 30339, United States*

ABSTRACT

On high-latitude continental margins sediment is supplied from land to the deep sea through a variety of processes, including iceberg and sea-ice rafting, and bottom current transport. The accurate reconstruction of sediment fluxes from these sources through time is important in palaeoclimate reconstructions. The goal of this study was to assess a shift in the intensity of glacial processes, iceberg and sea-ice rafting during the Pliocene through an investigation of coarse sediment deposited at the AND-2A site in the Ross Sea and at International Ocean Discovery Program Site U1359 on the Antarctic continental rise. Terrigenous particle-size distributions and suites of quartz grain microtextures in the sand fraction of the deep-sea sediments were compared to those from Antarctic glaciomarine diamictites as a baseline for proximal glacial sediment in its source area. Using images acquired through Scanning Electron Microscopy, and following a quantitative approach, fewer immature and potentially glacially transported grains were found in Pliocene deep-sea sand fractions than in ice-contact sediments. Specifically, in the lower Pliocene interval silt and fine sand percentages are elevated, and microtextures in at least half of the sand fraction are inconsistent with a primary glacial origin. Larger numbers of chemically altered and abraded grains in the deep-sea sand fraction, along with microtextures that are diagnostic of periglacial environments, suggest a role for eolian sediment transport. These results highlight the anomalous nature of high-latitude sediment fluxes during prolonged periods of ice-retreat. Furthermore, the identification of a significant offshore sediment flux during Antarctic deglaciation has implications for estimated nutrient supply to the Southern Ocean and the potential for high-latitude climate feedbacks under warmer climate states.

Keywords: Antarctica, microtexture, IRD, eolian

INTRODUCTION

Polar ice sheets are key variables in understanding the Earth's climate history. Traditionally, high-resolution sediment records of ice-rafted debris (IRD) have been widely used as a proxy for glacial activity. These records involve interpretations of sand-dominated coarse fraction fluxes to the deep-marine environment. Iceberg rafted debris upon its initial release is expected to have a similar composition to a till deposited directly from glacial ice. One approach is based on the assumption that the accumulation of debris with a grain diameter larger than 150 or 250 μm is proportional to the supply of glacially eroded coarse fraction from melting icebergs, a proxy called iceberg rafted debris (IBRD). Another is to use end-member modelling of grain-size distributions to assess IBRD abundance (Prins et al., 2002). Either approach implies that the supply of coarse debris by icebergs is constant in volume and size range and that all other processes that supply sand or coarser material to the deep sea are well-constrained. However, these conditions pose a challenge in analysing pre-Pleistocene stratigraphic records representing altered sediment fluxes under different climate states (Gilbert & Domack, 2003; Westerhold et al., 2020).

Here the transport history of the sand components recovered from Pliocene Antarctic drillcores is evaluated through detailed analyses of terrigenous particle-size distributions along with scanning electron microscopy (SEM) of quartz grain microtextures. Previous work has shown that high-resolution records of the abundance of coarse sand recovered from deep-sea drillcores on the Wilkes Land margin indicate a response to orbital forcing in the obliquity and precession bands (Patterson et al., 2014; Hansen et al., 2015). However, the contribution of the Neogene Antarctic Ice Sheet to global ice volume changes in the precession band is debated (DeVleesschouwer et al., 2017; Caballero-Gill et al., 2019), warranting investigation of the precise nature of the ice-rafted sediment fluxes (Gilbert, 1990).

An existing Pliocene high-resolution laser particle-size record (Hansen et al., 2015) from International Ocean Discovery Program (IODP) Site U1359 is extended across the Mid-Pliocene Warm Period (MPWP) and the relative proportions of the sand fluxes attributed to ice rafting and other sediment transport mechanisms for this deep-water site are investigated. Furthermore, a baseline for glacially derived material is provided by analyses of discrete intervals of Neogene ice-proximal diamictites recovered from the ANDRILL Site 2A (AND-2A) core in the Ross Sea (Fielding et al., 2008). The Ross Sea is considered to be the primary provenance area for Pliocene IBRD recovered from the Wilkes Land continental rise (Cook et al., 2017).

METHODS AND MATERIALS

The AND-2A drillhole was completed in 2007 in *ca* 380 m water depth on a sea-ice platform within 10 km of the East-Antarctic coast in the Ross Sea (Figure 1). In the upper *ca* 250 m, drilling recovered Neogene massive diamictites interbedded with minor stratified diamictites, sandstones and conglomerates (Passchier et al., 2011). Another interval of massive and stratified diamictite was recovered at *ca* 650 m below seafloor (mbsf). Based on macroscopic evidence of ice-proximal deposition, 46 samples were selected for particle-size analyses. Four diamictite intervals ranging from *ca* 6 to 14 m thick were selected for sampling at 0.5 to 1.0 m spacing to capture the vertical variability (Hansen, 2011). The selected intervals include diamictites with shear structures and clastic dikes, and range in age from Miocene to Pleistocene (Figure 2) (Fielding et al., 2008; Passchier et al., 2011).

The IODP Site U1359 was drilled in 4,003 m water depth within 100 km of the shelf break on the Wilkes Land margin and recovered Pliocene sediments between *ca* 50 and 150 mbsf (Figure 1). At Site U1359, as part of this study, 110 samples were analysed across the MPWP, and merged with the previously published record of Hansen et al. (2015). Pliocene sediments recovered at IODP Site U1359 consist primarily of silty clays and diatomaceous silty clays with dispersed clasts (>2 mm) with up to *ca* 43% biogenic silica (Hansen et al., 2015). Site U1359 was sampled at *ca* 3 kyr temporal resolution using an age model from Tauxe et al. (2012), which translated into a sample spacing of approximately 15 cm. Most samples were acquired from Hole U1359A. In one interval between 104.63 and 114.63 mbsf-A, where Hole U1359A had recovery gaps and poor core quality, equivalent strata were sampled in Hole U1359B (Hansen et al., 2015). Each sample consisted of an intact wedge of sediment from a *ca* 1.5 cm thick core interval, which was divided into subsamples prior to disaggregation.

Particle-size data

Particle-size distributions were measured on a Malvern Mastersizer 2000 laser particle-size analyser. The Udden-Wentworth grain-size classification was used (Wentworth, 1922). For indurated sediments, samples were first soaked in Millipore water to create a slurry. Samples were wet-disaggregated using a rubber cork, or pestle applying gentle vertical motion to the sample slurry to avoid breaking grains. Smear slides of samples were checked under a microscope to assess proper disaggregation before analysing them on the laser particle sizer. Ultrasonic treatment was used as a last resort to aid in the disaggregation. This process is labour-intensive, but has proven to be very effective given the excellent correlation between mud percent and geophysical properties data for the AND-2A core (Passchier et al., 2013, Geosphere, their figure 2B). To obtain the terrigenous fraction, organic matter and carbonate were digested through the addition of 30% H_2O_2 and 10% HCl to a 50-100 mL suspension on a hot plate. For IODP Site U1359, in order to assess the particle-size distribution of the siliciclastic sediment supplied from land, the data was collected on the terrigenous fraction of the marine sediment after dissolution of the biogenic silica, which typically consists of diatoms in the silt size range. Using data from the terrigenous fraction, allows for a direct comparison between particle-size distributions of ice-contact diamictite from the Antarctic continental shelf and the ice-distal sand fractions, including ice-rafted debris. Following centrifuge cycles to remove supernatant with excess chemicals, at Site U1359 biogenic silica was removed by mixing sediment with a 0.2 N NaOH solution in an 85-degree hot bath for one hour (Passchier, 2011). This standard method of wet-alkaline digestion is sufficient to remove most biogenic silica in hemipelagic sediments with low amounts of biogenic silica, while minimising loss of the lithogenic clay fraction (DeMaster, 1981; Ragueneau et al., 2005; Cardinal et al., 2007).

The Malvern Mastersizer 2000 is equipped with a Hydro 2000 MU wet sample dispersion unit. Prior to instrument analysis, the terrigenous fractions were dispersed using a heated sodium pyrophosphate solution. The Mastersizer 2000 uses Mie theory to provide calculations of the fine sediment fractions, which requires an estimate of the refractive index of the material. For the diamict samples, a standard operating protocol with refractive index 1.544 (quartz), absorption coefficient of 0.9, and rotor speed 2,200 rpm was followed. For the deep-marine samples, a refractive index of 1.6 (illite), absorption coefficient of 0.9 and rotor speed of 2,000 rpm was used. The rotor speed is a tradeoff between the proper dispersion of coarse materials and the increased incidence of air bubbles at higher rotor speeds. Other Malvern instrument variables were the same for all samples. Standard operating protocols are based on experiments with fine-grained sediments by Sperazza et al. (2004) and the authors own experiments with diamict aliquots. Quality control was performed through repeat analysis of a fine-grained industrial standard QAS3002 and an in-house natural fine sand standard (Sandy Hook Dune 4). Eight replicates of a fully dispersed till sample (D_{50}=25 μm; Uniformity= 3.4) show that results per 0.25 phi size class are typically reproducible within an uncertainty of <10%, as long as obscuration values are kept between 15 and 50 %. Eleven replicates of the coarser dune standard (D_{50}=354 μm; Uniformity= 0.3) show a typical relative uncertainty of <15% per 0.25 phi size class. However, larger relative uncertainty is observed at the edges of the grain-size distributions, where there is a large difference in vol. % between two adjacent size classes.

SEM analysis of quartz grain microtextures

For the microtexture analysis, 786 SEM images of quartz grains from sieved > 63 μm sand fractions of 20 samples were examined, 10 from each site. In the ANDRILL core, SEM samples were chosen based on their proximity to shear structures or other evidence of ice-contact deposition (Hansen, 2011; Table 1; Figure 2). At Site U1359, samples with large quantities of terrigenous sand and some samples with lower quantities were selected for SEM analysis to investigate the sediment transport history for the sand fraction (Hansen, 2016; Rosenberg, 2014; Table 1; Figure 3). Samples were wet-sieved over 63 µm and *ca* 40 grains were picked quickly and without examination from the >63 µm fraction. The vast majority of the grains that were picked were in the 200-500 µm size range. All grains were coated with a thin layer of gold-palladium. The images were created in secondary electron (SE) mode at 12kV with a *ca* 10 mm working distance on a Hitachi S3400N Scanning Electron Microscope at the Microscopy and Microanalysis Research Laboratory (MMRL) at Montclair State University. Grain composition was checked using a Bruker X-Flash energy dispersive X-ray spectrometer (EDS) system and only the 786 grains that had a SiO_2 composition were analysed for microtextures. A quantitative approach to microtexture analysis was used, focusing on combinations of microtextures on individual grains for palaeoenvironmental interpretations (Hodel et al., 1988; Dunhill, 1998; Mahaney et al., 2001; Damiani et al., 2006; Hart, 2006; Cowan et al., 2014).

Initially, the observation and characterisation of individual microtextures involved comparison of textures on grains of unknown origin to grains from known sedimentary environments (Helland & Holmes, 1997; Mahaney, 2002 and other references therein). Microtextures were observed visually following a checklist by the second author (Hansen, 2011, 2016). The work on each site was part of a different project. The checklists for each of the palaeoenvironments were slightly different because of variability in the microtextures that were encountered in the samples derived from the diamictites versus the glacially influenced deep-marine environment.

In a sensitivity study, Culver et al. (1983) demonstrated that operator variance existed in the classification of individual microtextures, but also that the environmental interpretations based on blind surveys of sets of multiple microtextures on each grain, along with grain roundness and relief, were consistent and accurate for five different operators. Therefore, the use of combinations of microtextures is preferred in environmental discrimination (Mahaney et al., 2001). Furthermore, the presence of grains recycled from pre-existing sediments and sedimentary rocks can create a strong provenance-related overtone in the texture tallies in studies of glacial environments (cf. Mazullo & Ritter, 1991). To avoid this problem, observations on the various layers of textures that overprint each other are also made on the entire grain surface with the aim to separate textures produced during the multiple cycles of surface exposure, erosion, sediment transport and deposition (cf. Mahaney et al., 2001; Molén, 2014; Woronko & Pisarska-Jamroży, 2016). In the workflow of SEM studies of quartz grain populations, it is uncommon that microtextures are observed separately from the context of the entire grain, including its other textures and the grain shape. Therefore, the microtextures that are tallied for each grain are typically not independent observations and, in such cases, the use of statistical methods on microtexture checklists to underpin environmental interpretations is not a valid approach.

For these reasons, SEM images were reanalysed by the first author to classify grains visually into grain types, with criteria established based on expected source-to-sink sediment transport histories and with emphasis on the multi-cyclic nature of sediment transport before deposition (Mahaney et al., 2001; Molén, 2014). Individual grains were attributed to one of 12 grain types based on a survey of combinations of microtextures, grain roundness, and relief. Each of the 12 grain types was interpreted as a product of a specific sediment transport path and depositional environment based on the genetic interpretation of combinations of microtextures, and how textures overprinted each other on the surfaces of the grains.

Image file ID names and grain sources were randomised using a script prior to analysis and the origin of each image, i.e. which AND-2A or U1359 core sample, was unknown to the operator to avoid subconscious bias. The entire batch of 786 grains was classified into grain types before image file names were reinstated. This process created a raw dataset with 786 completely independent observations. Prior to analysis, values were standardised by dividing the frequency for each grain type by the average frequency for that grain type. The statistical analysis was carried out with the Principal Coordinates Analysis module using Bray-Curtis Similarity with a transformation coefficient of 2 in PAST v. 3.26b (Hammer et al., 2001). The algorithm is from Davis (1986). The Bray-Curtis Similarity was chosen over the Euclidian Distance or other methods because of its better handling of 'zero' counts in observations. Principle Coordinates Analysis is more commonly known as Metric Multidimensional Scaling (MDS) and is used to determine whether a collection of observations represents a single population or a mixture of several populations.

RESULTS AND INTERPRETATIONS

Particle-size distributions show variability in sand content in the four densely sampled intervals of Miocene, Pliocene and Pleistocene diamictites in the AND-2A core in the Ross Sea (Figure 1). Stratified muddy diamict (at 648-663 and 238-250 mbsf) is homogeneous over a depth range and predominantly silt-rich, consisting of gravel-sized (> 2-mm diameter) clasts within a matrix of glacial rock flour (Figure 1). In contrast, Upper Miocene to Pleistocene massive diamictites (134-142 and 64-70 mbsf) show both fine and coarse-sand modes, even in repeat analysis of the same samples. Such till matrix heterogeneity can be attributed to differences in the efficiency of glacial comminution processes, where grain crushing dominates over abrasion under high effective pressures (Hiemstra & Van der Meer, 1997; Cowan et al., 2014). At deep-water Site U1359, coarse sand dominates the >125 µm dispersed sand fraction in the upper Pliocene section (Figure 4A), with a complete absence of fine sand in the entire interval sampled between 48 and 70 mbsf (Figures 1 and 4B). In contrast, lower Pliocene hemipelagic and diatom-rich silty clays have variable terrigenous grain-size distributions with mostly fine-sand modes and only occasionally coarse sand (Figure 4C,D).

Observations of number of grains carrying each microtexture in each of the checklists for sample intervals and individual samples are tallied here as bar graphs (Figure 5). Noteworthy is that fractured plates are present on >50% of grains and v-shaped impact pits on >25% of grains in the diamictites, along with microtextures, such as straight and arcuate steps, conchoidal fractures and grooves. Grains exhibiting upturned plates and mechanical impact microtextures, such as impact craters, chattermarks, abrasion features and rounded edges were observed in the samples from the glacially influenced deep-marine environment (Site U1359).

In the reanalysis, 12 grain types were distinguished based on the examination of co-existing microtextures on each grain (Figure 6 and Table 2). Samples within close proximity in a core interval, are plotted together in the histograms, and have similar grain-type distributions (Figure 7). Modified glacially derived grains with high relief, steps, parallel fractures, conchoidal fractures, microblocks and edge rounding (Type D) were the most common grain type found overall at both sites (Figures. 7 and 8). In contrast, low-medium relief subrounded to rounded grain types G and H (Figure 6), which resemble those found in lowland rivers such as the Nile and Loire (Manickam & Barbaroux, 1987; Vos et al., 2014) were rare in these Antarctic samples.

Medium relief rounded grains with v-shaped and dish-shaped percussion marks, conchoidal fractures and grain breakage (Type F), indicative of high-intensity subaqueous transport are also rare, except for one interval of sandy diamictite in AND-2A at 250.11 m, and one interval above a normally graded lamina in U1359 at *ca* 62 mbsf (sample U1359A-8H4). Not unexpectedly, the diamictites from the Ross Sea continental shelf exhibited the largest proportion of high-relief angular Type C grains with steps, parallel fractures, conchoidal fractures or microblocks (Figure 8), surface textures that are found on grains from modern and recent glacial environments (Whalley & Krinsley, 1974; Whalley & Langway, 1980; Hodel et al., 1988; Mahaney et al., 1996; Molén, 2014). In contrast, Type I grains that are almost entirely covered with polygenetic upturned plates, saw-tooth fractures or broken plates (Figure 9) are surprisingly abundant in deep-marine sediments at Site U1359, but rare in the diamictites (Figure 7A). The hemipelagic sediments also contain common high-relief Type E grains with smoothed/abraded fracture surfaces, dish-shaped depressions, edge rounding and precipitation (Figure 9). These grain types are found in periglacial or high elevation desert environments where perennial lake, river and/or eolian sediment transport processes are impacting otherwise immature quartz grains (Margolis & Krinsley, 1971; Wellendorf & Krinsley, 1980; Woronko & Hoch, 2011; Shrivastava et al., 2014; Mahaney, 2015; Kalińska-Nartiša et al., 2017; Hao et al., 2019; Li et al., 2020).

The MDS statistical analysis reveals a correlation between macroscopically defined sedimentary facies and microtextures (Figure 7B). The first two coordinates explain 51% of the variance. Samples plotting near each other on the ordination plot are more similar to each other than samples plotting far away from each other. Diamicts plot in a narrow range on the first coordinate axis (MDS 1) with limited overlap between massive and stratified diamicts. Most deep-water samples plot in a narrow range on the second coordinate axis (MDS 2; Figure 7B).

However, upper Pliocene samples from IODP Site U1359, including sample U1359A-7H4-90-92, have greater similarity in grain microtextures to stratified diamicts than lower Pliocene samples, as is also evident from the grain type frequency distributions (Figure 7A). The least similar samples to diamictites are from Cores U1359B-13H and U1359A-15H. Samples from these cores also yielded 5 grains of altered and abraded vesicular glass as part of the sand fraction investigated via SEM analysis (Figure 10).

DISCUSSION

To investigate the relative importance of Pliocene iceberg rafting from the Ross Sea as a sediment dispersal mechanism of coarse sediment, suites of quartz grain microtextures are compared between glacially influenced IODP Site U1359 on the Antarctic Wilkes Land continental rise and its IRD source represented by the AND-2A diamictites. Subsequently, sand fluxes are evaluated using terrigenous particle-size distributions.

Microtexture frequencies

One challenge with the environmental interpretation of raw frequencies of quartz grain microtextures (Figure 5) is the strong provenance signal in the texture distributions in grains from glacial environments (Moss & Green, 1975; Mazullo & Ritter, 1991). In Cenozoic tills deposited in valleys in the uplands of the Transantarctic Mountains, conchoidal and sublinear fractures are abundant, and v-shaped impact pits are also present (Mahaney et al., 1996). In samples of AND-2A diamictites the high frequencies of fractured plates, breakage blocks, in addition to v-shaped impact pits (Figure 5) points to glacial erosion and transport of quartz derived from crystalline and/or immature sedimentary rocks (Mazullo & Ritter, 1991). Rounding of grains and an increase in v-shaped impact pits on glacially sourced grains have been observed elsewhere after only *ca* 80 km of subaqueous transport (Sweet & Brannan, 2016). However, in this study these textures are more consistent with inheritance of grain morphologies through glacial erosion in the lower crystalline basement and fluvio-deltaic sections of the Beacon Supergroup of the Transantarctic Mountains (Panter et al., 2008). Glacial entrainment through plucking under the edge of a thinner polythermal icesheet and the active tectonics may have contributed to the presence of a relatively large component of inherited textures on grains from AND-2A diamictites.

In the samples from the glacially influenced deep-marine environment (Site U1359), more grains exhibited upturned plates and mechanical impact microtextures, such as impact craters, chattermarks, abrasion features, saw-tooth fractures and rounded edges (Figure 5). These textures are more consistent with transport in different kinds of flows by wind and water (Lindé & Mycielska-Dowgiałło,1980; Costa et al. 2013). The microtexture checklist surveys show differences in the observed frequency distributions of microtextures per sample between ice-contact diamictites and glacially influenced deep-marine sediments with evidence of ice rafting. In sediment transport from source to sink, the likelihood that the original texture inherited from the source rock is preserved decreases, unless grains stay embedded in the glacial ice or an iceberg until deposition.

Grain-type classification and palaeoenvironmental interpretation

The classification of entire grain surfaces allows for the characterisation of multiple consecutive sediment transport modes and palaeoenvironment (Table 2). This is achieved by separating the inherited from contemporaneous textures within the context of how textures coexist and overprint each other on individual grains (Molén, 2014). Sand dispersal to the Antarctic continental rise takes place as iceberg rafted debris (IBRD), sea-ice rafted debris (SIRD) and hyperpycnal flows (Damiani et al., 2006; Cowan et al., 2008; Patterson et al., 2014; Hansen et al., 2015). Sediment can be supplied to sea ice through eolian transport, as freeze-on, anchor ice floatation, frazil ice formation and wash overs (Powell & Domack, 2002). Grain types recovered from subglacial tills, i.e. the AND-2A massive diamictites with shear structures, represent the population in the ice source for ice rafting, and modification of grain surfaces by eolian and subaquatic sediment transport is expected in the proglacial or glaciomarine environment (Hodel et al., 1988; Dunhill, 1998; Sweet & Brannan, 2016, Kalińska-Nartiša et al., 2017).

In deep-marine sediment samples from Site U1359, between 23 and 58% of grains have either fresh or modified glacial microtextures, such as steps, parallel and/or conchoidal fractures, or microblocks (Types B, C and D; Figure 8), compared to between 48 and 75% of grains in the Ross Sea diamictites (Figure 7). The lower number of grains with primary glacial microtextures (Types B, C and D) than the baseline ice-proximal diamictite is inconsistent with a sole IBRD source for the sediment at deep-marine Site U1359. Between 6 and 39% of grains from the deep-water site are of Type I and have textures, such as upturned plates and saw-tooth fractures with dissolution (Figure 9). In contrast, Type I grains were rare (<10 %) in the survey of diamicts from the AND-2A core. Upturned plates were also rare in tills from the Transantarctic Mountains (Mahaney et al., 1996).

Only a low abundance of grains with mechanical impact textures are present in the upper Pliocene samples in Cores 7H, 8H and 9H. The upper Pliocene continental rise samples contain common grains of the glacial grain types B, C and D, and, as a result plot in the MDS near the glaciomarine stratified diamictites from the continental shelf (Figure 7B). It is possible that glacial transport followed by minor current or wave impact on some grains produced similar grain types in both the continental shelf and deep-water glaciomarine settings. These comparisons suggest that the sand fractions retrieved from the upper Pliocene interval represent IBRD from ice sheets entraining material similar to shelf diamictites prior to calving.

On the other hand, samples from lower Pliocene diatom-rich silty clays with dispersed gravel in Cores U1359B-13H and U1359A-15H are distinct in their microtexture distributions as is also evident from the position of these samples on the MDS plot (Figure 7). Chemically rounded grains (Types E and G), and grains with saw-tooth fractures and upturned plates (Type I) represent between 30 and 70% of grains in these samples, whereas the percentages for these grain types combined are < 20% in the diamictites. Silt and fine sand laminae (example in Figure 3E) are present in the lower Pliocene interval of Site U1359 (Figure 1B). Smear slides show that some laminae also contain diatom debris and are not completely clastic (Expedition 318 Scientists, 2011). Given the lack of evidence for subaqueous bedload transport in the microtextures, along with the reduced terrigenous, and the elevated diatom-component in the sediment, only winnowing or suspension transport as part of density flows could have been responsible for the development of the laminae. Furthermore, Hansen et al. (2015) pointed out that, locally, sand and gravel-sized coarse fraction is dispersed within the graded laminated mud facies in this interval, which was explained by a combination of iceberg rafting and sediment lofting from hyperpycnal flows. Since microtextures that would support bedload transport by bottom currents, such as v-shaped impact pits, are lacking, it is assumed that sediment was deposited after transport in suspension or via gravity settling only. Chemical smoothing and rounding and upturned plates are generally attributed to in-situ weathering, cryoturbation, and eolian transport under a periglacial setting, which must have taken place prior to transport to the deep sea (Moss & Green, 1975; Wellendorf & Krinsley, 1980; Woronko & Hoch, 2011).

Microtextures consistent with preweathering and edge rounding induced by subaerial surface processes were also found by Cowan et al. (2008) on quartz grains from Pliocene continental rise sediments off the Antarctic Peninsula. There, the grains that lacked features of glacial transport were interpreted as supraglacial debris supplied by iceberg-calving from a thinner Pliocene ice sheet, with greater exposure of glacial valley walls. Supraglacial debris is not well-documented on top of the outlet glaciers and ice streams in the Ross Sea. However, isolated drapes of sorted eolian sand have been described from Wright Glacier in the Dry Valleys and other areas (Hambrey & Glasser, 2012). In the Ross Sea, eolian sediment with a prominent fine sand mode is also observed to collect onto sea ice near-shore, and it is derived from the McMurdo Ice Shelf (Atkins & Dunbar, 2009). For a warmer climate setting in the Antarctic Peninsula region, Gilbert and Domack (2003) explain the origin of eolian sediment on the seafloor through the deposition of wind-blown sediment in melt ponds on top of ice shelves and release of eolian sediment at the onset of ice-shelf break-up as the melt ponds drain. Therefore, for sediment sourced from the Ross Sea embayment during the warm Pliocene eolian sediment transport followed by either iceberg or sea-ice rafting can be regarded as a viable transport mechanism for portions of the sand fraction found offshore.

Eolian sediment supply

The quartz component of modern pelagic sediment deposited away from fluvial sources is typically of eolian origin (Leinen et al., 1986; Hodel et al., 1988). The largest proportions of wind-blown sediment occur offshore sourced from unvegetated regions, typically deserts, and areas of deposition reflect the dominant wind patterns. Today, Antarctica's periglacial surfaces have limited exposure due to extensive glaciation, which limits eolian sand supply. In the modern Ross Sea, eolian sediment concentrations on sea ice are observed to be low more than 15 km offshore although some wind-blown sand can be transported large distances (> 100 km) over sea ice via saltation during high-wind events (Chewings et al., 2014).

The annual eolian sediment flux can be expected to be a function of sediment availability and wind regime and these boundary conditions were markedly different during the early Pliocene in this area of Antarctica. East Antarctic ice retreat exposed larger areas of East Antarctica within the Wilkes and Aurora Subglacial basins that were elevated above sea level due to glacio-isostatic rebound and differences in dynamic topography (Cook et al., 2013; Austermann et al., 2015; Dumitru et al., 2019) (Figure 1C). The bulk geochemistry of Pliocene sediments from IODP Site U1358 on the Wilkes Land continental shelf shows limited chemical weathering of the mudrocks (Orejola et al., 2014), implying that the Antarctic source areas were cold and arid despite the deglaciation. Compared to modern seafloor sediments, Pliocene dispersed sand on the Wilkes Land margin contains a large proportion of quartz (Cook et al., 2017) and quartz is particularly resistant to the extreme attrition of grains in eolian transport. Furthermore, atmospheric modelling shows that upon deglaciation in the Pliocene, Site U1359 was in the pathway for eolian transport from the exposed source terrains with seasonally averaged summer wind speeds in excess of 10 m/s extending across the ocean surface (Scherer et al., 2016). During high wind events, wind speeds were probably sufficient to entrain sand under dry conditions and transport it onto ice shelves or over a sea-ice surface via saltation (Gilbert, 1990; Gilbert & Domack, 2003; Chewings et al., 2014).

Modern conditions in the Ross Sea are unlikely to be representative of past interglacials with the exposure of emerging coasts as discussed above. Therefore, the modern interglacial setting of the glaciated Canadian shield is used as an additional partial analogue for the early Pliocene interglacials. Field experiments on a modern emerging coastline in eastern Canada show that, under dry conditions with unlimited supply, fine to medium sand is typically mobile at wind speeds of 10 m/s (Davidson-Arnott et al., 2008). At higher latitude, eolian sediment transport is evident in the Arctic Coastal Plain of Alaska, where large sand dunes have formed through thermokarst, wind erosion and transport of exposed Pleistocene marine sediments (Carter, 1981). Furthermore, North of Alaska, eolian sediments contribute a large proportion of the sand fraction on the continental shelf and half the grains in a sample of frazil ice in this region were found to have rounding and textures typical of eolian transport histories (Hodel et al., 1988). Microtextures on grains retrieved from modern Arctic sea ice floes also show common edge rounding, silica dissolution and precipitation, upturned plates and microlayering (described as mechanical and chemical layer separation), in addition to microtextures typical of glacial sediments, such as conchoidal and step-like fractures, striations, gouges and breakage blocks (Dunhill et al., 1998; St. John et al., 2015). These microtexture populations are also indicative of a combination of glacial, periglacial and eolian processes (Moss & Green, 1975; Wellendorf & Krinsley, 1980; Woronko & Hoch, 2011).

At IODP Site U1359, Hansen et al. (2015) interpreted a concentration of gravel (> 2mm) at *ca* 4.5 Ma as a pulse of iceberg rafted debris due to calving, followed by glacial retreat. However, comparison of grain-size distributions and microtextures with ice-proximal diamictites in the source area, indicate that approximately half of the sand grains in this interval were supplied through eolian sediment transport. It is envisioned that sediment was entrained or transported onto ice shelves or sea ice near the coast, with wind-driven sea-ice drift (Holland & Kwok, 2012; Chewings et al., 2014), followed by iceberg and sea-ice rafting and deposition at Site U1359. Sediment may have been eroded and transported by glaciers initially, followed by exposure, entrainment and modification in subaerially exposed periglacial environments or while embedded in the ice shelves, icebergs, or sea ice. Even though this scenario could imply a different provenance for this microtextural group as compared to the IBRD from the Ross Sea, a different provenance alone cannot explain the pervasive alteration of grain surfaces observed via SEM.

Export to the sea floor on the continental rise may have occurred via settling through the water column upon tipping of icebergs releasing their supraglacial load, from seasonal sea ice via transport from the continental shelf through high-density saline flows originating from a shelf polynya, or wind-driven circulation. The exact mechanisms remain uncertain. Ice shelf and sea-ice palaeorecords are sparse for the early Pliocene and indicate some spatial and temporal variability in extent (Whitehead et al., 2005; Taylor-Silva & Riesselman, 2018). Nevertheless, regardless of the exact scenario, the early Pliocene increase in the offshore sediment supply in the silt and sand fraction may have been primarily governed by the eolian sediment fluxes and not rates of iceberg calving, even in the presence of concentrations of gravel-sized IBRD.

Broader implications

The implications of this finding are twofold. First, these results confirm challenges in using different grain-sizes in the sand fraction as a proxy for glacial activity (Gilbert, 1990). The glacial sediment load in icebergs as characterised by the multimodal particle-size distributions of diamictites, can be expected to have a variable sand mode (Figure 1A). Furthermore, with glacial retreat the contribution of periglacial sediment cannot be ignored in the deposition of hemipelagic sediment with IRD. Dunhill (1998) noted that the unique property of IBRD in the modern Arctic is the presence of gravel, which is absent from SIRD. Therefore, gravel abundances are probably the most reliable first-order proxy for iceberg flux in continental margin settings where multiple sediment fluxes operate concurrently, whereas particle-size distributions and microtexture studies illuminate the nature of the other sediment fluxes.

Second, the discovery of enhanced wind-driven nutrient fluxes to the surface ocean could alter discussions of the biological carbon pump and other carbon cycle perturbations originating in the Southern Ocean during periods of deglaciation (Chewings et al., 2014; Caballero-Gill et al., 2019). Southern Ocean productivity is severely nutrient-limited with nutrient supply from sources outside Antarctica focused during glacials, not periods of ice retreat. This study highlights a different scenario for the past, during the Pliocene Climatic Optimum, when the Earth system operated under a different climate state (Westerhold et al., 2020).

CONCLUSIONS

It has been demonstrated here using a combination of sedimentological techniques that Pliocene dispersed sand within deep-marine sediments off the Wilkes Land margin, Antarctica, in comparison to diamictites with the same source, can contain a substantial non-glacial component. In contrast to the upper Pliocene IBRD, the lower Pliocene sand fraction has a distinct character with a larger silt to fine sand mode and a proportion of grains that are chemically weathered or exhibit polygenetic upturned plates. These types of grains are found predominantly in periglacial environments where frost-weathering and eolian sediment transport processes prevail (Margolis & Krinsley, 1971; Woronko & Hoch, 2011). The lower Pliocene

IRD maxima partially represent enhanced eolian fine sand fluxes via sea ice or supraglacial debris in icebergs with a possible role for export through density flows, but not bedload transport. Separating IBRD, the supraglacial component, and SIRD by grain-size alone is difficult: the variable sand modes of ice-proximal diamictites show that IBRD pulses can be misinterpreted when gravel counts and the fine sand fraction are omitted from the proxy. Microtexture analyses of quartz grains, in addition to particle-size analysis, and gravel counts provides greater insight into the relative contributions of sediment fluxes in a glaciomarine environment, and enhances the accuracy of palaeoclimate reconstructions.

DATA

Particle-size data for diamictite intervals in AND-2A: https://doi.org/10.15784/601452

Particle-size data for Site U1359: https://doi.org/10.15784/601450

The other data that support the findings of this study are available from the corresponding author upon reasonable request.

ACKNOWLEDGMENTS

Samples for this research were provided by the International Ocean Discovery Program (IODP) and the Antarctic Drilling Program (ANDRILL). Financial support was provided by U.S. National Science Foundation awards ANT 0838842, OCE 1060080, and ANT 1743643 to S. Passchier. Drs. Stefanie Brachfeld and Laying Wu are thanked for their technical assistance in the SEM Lab. Dustin Sweet, Bill Mahaney, Mats Molén, Nick Eyles and three anonymous reviewers are thanked for their feedback.

REFERENCES CITED

Atkins, C. B., and Dunbar, G. B. (2009) Aeolian sediment flux from sea ice into Southern McMurdo Sound, Antarctica. *Global and Planetary Change*, 69(3), 133-141.

Austermann, J., Pollard, D., Mitrovica, J. X., Moucha, R., Forte, A. M., DeConto, R. M., Rowley, D. B., and Raymo, M. E. (2015) The impact of dynamic topography change on Antarctic ice sheet stability during the mid-Pliocene warm period. *Geology*, 43(10), 927-930.

Caballero-Gill, R. P., Herbert, T. D., and Dowsett, H. J. (2019) 100-kyr paced climate change in the Pliocene warm period, Southwest Pacific. *Paleoceanography and Paleoclimatology*, 34, 524–545.

Cardinal, D., Savoye, N., Trull, T. W., Dehairs, F., Kopczynska, E. E., Fripiat, F., Tison, J.L. and André, L. (2007) Silicon isotopes in spring Southern Ocean diatoms. Large zonal changes despite homogeneity among size fractions. *Marine Chemistry*, 106(1-2), 46-62.

Carter, L. D. (1981) A Pleistocene Sand Sea on the Alaskan Arctic Coastal Plain. *Science*, 211(4480), 381-383. Available at: doi:10.1126/science.211.4480.381.

Chewings, J.M., Atkins, C.B., Dunbar, G.B. and Golledge, N.R. (2014) Aeolian sediment transport and deposition in a modern high-latitude glacial marine environment. *Sedimentology*, 61. 1535-1557. Available at: doi:10.1111/sed.12108.

Cook, C. P., van de Flierdt, T., Williams, T., Hemming, S.R., Iwai, M., Kobayashi, M., Jimenez-Espejo, F.J., Escutia, C., Gonzalez, J.J., Khim, B.-K., McKay, R.M., Passchier, S., Bohaty, S.M., Riesselman, C.R., Tauxe, L., Sugisaki, S., Galindo, A. L., Patterson, M. O., Sangiorgi, F., Pierce, E.L., Brinkhuis, H., and IODP Expedition 318 Scientists (2013)

Dynamic behaviour of the East Antarctic Ice Sheet during Pliocene warmth. *Nature Geoscience*. Available at: doi: 10.1038/ngeo1889.

Cook, C. P, Hemming, S.R., van de Flierdt, T., Pierce Davis, E., Williams, T.R., López Galindo, A., Jiménez-Espejo. F.J., and Escutia, C. (2017) Glacial erosion of East Antarctica in the Pliocene. A comparative study of multiple marine sediment provenance tracers. *Chemical Geology*, 466, 199-218.

Costa, P. J. M., Andrade, C., Mahaney, W. C., Da Silva, F. M., Freire, P., Freitas, M. C., Janardo, C., Oliveira, M. A., Silva, T., and Lopes, V. (2013) Aeolian microtextures in silica spheres induced in a wind tunnel experiment: Comparison with aeolian quartz. *Geomorphology*, 180, 120-129.

Cowan, E.A., Hillenbrand, C.D., Hassler, L.E. and Ake, M.T. (2008) Coarse-grained terrigenous sediment deposition on continental rise drifts: A record of Plio-Pleistocene glaciation on the Antarctic Peninsula. *Palaeogeography, Palaeoclimatology, Palaeoecology*, 265(3-4), 275-291.

Cowan, E.A., Christoffersen, P., Powell, R.D. and Talarico, F.M. (2014) Dynamics of the late Plio–Pleistocene West Antarctic Ice Sheet documented in subglacial diamictites, AND-1B drill core. *Global and Planetary Change*, 119, 56-70.

Culver, S.J., Bull, P.A., Campbell, S., Shakesby, R.A., and Whalley, W.B. (1983) Environmental discrimination based on quartz grain surface textures: a statistical investigation. *Sedimentology*, 30, 129-136.

Damiani, D., Giorgetti, G., and Turbanti, I. M. (2006) Clay mineral fluctuations and surface textural analysis of quartz grains in Pliocene–Quaternary marine sediments from Wilkes

Land continental rise (East-Antarctica): Paleoenvironmental significance. *Marine Geology*, 226(3-4), 281-295.

Davidson-Arnott, R. G. D., Yang, Y., Ollerhead, J., Hesp, P. A., and Walker, I. J. (2008) The effects of surface moisture on aeolian sediment transport threshold and mass flux on a beach. *Earth Surface Processes and Landforms*, 33(1), 55-74.

Davis, J.C. (1986) Statistics and Data Analysis in Geology. John Wiley & Sons.

DeMaster, D.J. (1981) The supply and accumulation of silica in the marine environment. *Geochimica et Cosmochimica Acta*, 45, 1715–1732.

De Vleeschouwer, D., Vahlenkamp, M., Crucifix, M., and Pälike, H. (2017) Alternating Southern and Northern Hemisphere climate response to astronomical forcing during the past 35 m.y. *Geology*, 45(4), 375-378.

Dunhill, G. (1998) Comparison of Sea-ice and Glacial-ice Rafted Debris: Grain Size, Surface Features, and Grain Shape. *U.S. Geological Survey Open-File Report* 98-367, 80p.

Dumitru, O. A., Austermann, J., Polyak, V. J., Fornos, J. J., Asmerom, Y., Gines, J., Gines, A., and Onac, B. P. (2019) Constraints on global mean sea level during Pliocene warmth. *Nature*, 574(7777), 233-236.

Expedition 318 Scientists (2011) Site U1359. In Escutia, C., Brinkhuis, H., Klaus, A., and the Expedition 318 Scientists, *Proc. IODP, 318*, Tokyo (Integrated Ocean Drilling Program Management International, Inc. Available at: doi:10.2204/iodp.proc.318.107.2011.

Fielding, C.R., Atkins, C.B., Bassett, K.N., Browne, G.H., Dunbar, G.B., Field, B.D., Frank, T.D., Krissek, L.A., Panter, K., Passchier, S., Pekar, S.F., and the ANDRILL-SMS Science Team (2008) Sedimentology and stratigraphy of the AND-2A core, ANDRILL Southern McMurdo Sound, Project, Antarctica. *Terra Antartica*, 15, 77-112.

Gilbert, R. (1990) Rafting in glacimarine environments. *Geological Society, London, Special Publications*, 53(1),105-120.

Gilbert, R., and Domack, E.W. (2003) Sedimentary record of disintegrating ice shelves in a warming climate, Antarctic Peninsula. *Geochemistry, Geophysics, Geosystems*, 4(4), Available at: doi:10.1029/2002GC000441.

Hambrey, M.J., and Glasser, N.F. (2012) Discriminating glacier thermal and dynamic regimes in the sedimentary record. *Sedimentary Geology*, 251–252, 1-33, Available at: doi:10.1016/j.sedgeo.2012.01.008.

Hammer, Ø., Harper, D.A.T., and P. D. Ryan (2001) PAST: Paleontological Statistics Software Package for Education and Data Analysis. *Palaeontologia Electronica*, 4(1): 9pp.

Hansen, M.A. (2011) Determining middle Miocene through Pliocene changes in provenance and basal ice conditions through sedimentological analyses of subglacial diamictites in AND-2A, Ross Sea, Antarctica. M.S. Thesis, Montclair State University, Dept. of Earth and Environmental Studies.

Hansen, M.A. (2016) An assessment of Antarctic ice sheet dynamics from a Pliocene polar paleoclimate archive. Ph.D. dissertation, Montclair State University, Dept. of Earth and Environmental Studies.

Hansen, M. A., Passchier, S., Khim, B.-K., Song, B., and Williams, T. (2015) Threshold behavior of a marine-based sector of the East Antarctic Ice Sheet in response to early Pliocene ocean warming. *Paleoceanography*, 30(6), 789-801.

Hao, L., Tao, H., Guo, R., Mou, W., Tian, B., & Ma, X. (2019) Hydrodynamic evolution from quartz microtextures of a beach ridge in Qinghai Lake, China. *Sedimentary Geology*, 389, p. 13-25.

Hart, J.K. (2006) An investigation of subglacial processes at the microscale from Briksdalsbreen, Norway. *Sedimentology*, 53: 125-146, doi:10.1111/j.1365-3091.2005.00758.x

Helland, P.E. and Holmes, M.A. (1997) Surface textural analysis of quartz sand grains from ODP Site 918 off the southeast coast of Greenland suggests glaciation of southern Greenland at 11 Ma. *Palaeogeography, Palaeoclimatology, Palaeoecology*, 135, p. 109-121.

Hiemstra, J. F., and Van der Meer, J. (1997) Pore-water controlled grain fracturing as an indicator for subglacial shearing in tills. *Journal of Glaciology*, 43(145), 446-454.

Hodel, K. L., Reimnitz, E., and Barnes, P. W. (1988) Microtextures of quartz grains from modern terrestrial and subaqueous environments, north slope of Alaska. *Journal of Sedimentary Petrology*, 58(1), 24-32.

Holland, P.R. and R. Kwok (2012) Wind-driven trends in Antarctic sea-ice drift. *Nature Geoscience*, 5(12), 872-875.

Kalińska-Nartiša, E., Lamsters, K., Karušs, J., Krievāns, M., Rečs, A., and Meija, R. (2017) Quartz grain features in modern glacial and proglacial environments: A microscopic study from the Russell Glacier, southwest Greenland. *Polish Polar Research*, 38(3), 265-289.

Leinen, M., Douglas, C., Heath, G. R., Biscaye, P. E., Kolla, V., Thiede, J., and Dauphin, P. (1986) Distribution of biogenic silica and quartz in recent deep-sea sediments. *Geology*, 14, 199-203.

Li, Z., Yu, X., Dong, S., Chen, Q., and Zhang, C. (2020) Microtextural features on quartz grains from eolian sands in a subaqueous sedimentary environment: A case study in the hinterland of the Badain Jaran Desert, Northwest China. *Aeolian Research*, 43.

Lindé, K., & Mycielska-Dowgiałło, E. (1980) Some experimentally produced microtextures on grain surfaces of quartz sand. *Geografiska Annaler: Series A, Physical Geography*, 62(3-4), 171-184.

Mahaney, W. C., Claridge, G., and Campbell, I. (1996) Microtextures on quartz grains in tills from Antarctica. *Palaeogeography Palaeoclimatology Palaeoecology*, 121, 89-103.

Mahaney, W.C., Stewart, A. and Kalm, V. (2001) Quantification of SEM microtextures useful in sedimentary environmental discrimination. *Boreas*, 30, 165-171, Available at: doi:10.1111/j.1502-3885.2001.tb01220.x.

Mahaney, W. C. (2002) Atlas of sand grain surface textures and applications. Oxford University Press, USA.

Mahaney, W. C. (2015) Pedological iron/Al extracts, clast analysis, and coleoptera from Antarctic Paleosol 831. evidence of a Middle Miocene or earlier climatic optimum. *The Journal of Geology*, 123(2)), 113-132.

Manickam, S., and Barbaroux, L. (1987) Variations in the surface texture of suspended quartz grains in the Loire River: an SEM study. *Sedimentology*, 34, p. 495-510.

Margolis, S. V., and Krinsley, D. (1971) Submicroscopic Frosting on Eolian and Subaqueous Quartz Sand Grains. *Geological Society of America Bulletin*, 82, 3395-3406.

Mazullo, J. and Ritter, C. (1991) Influence of sediment source on the shapes and surface textures of glacial quartz sand grains. *Geology* 19 (4), 384–388. Available at: doi: 10.1130/0091-7613(1991)019<0384:IOSSOT>2.3.CO;2.

Molén, M. O. (2014) A simple method to classify diamicts by scanning electron microscope from surface microtextures. *Sedimentology*, 61(7), 2020-2041.

Moss, A. J., and Green, P. (1975) Sand and silt grains: Predetermination of their formation and properties by microfractures in quartz. *Journal of the Geological Society of Australia*, 22(4), 485-495.

Orejola, N., Passchier, S., and Expedition 318 Scientists (2014) Sedimentology of lower Pliocene to Upper Pleistocene diamictons from IODP Site U1358, Wilkes Land margin, and implications for East Antarctic Ice Sheet dynamics. *Antarctic Science*, 26(02), 183-192.

Panter, K.S., Talarico, F.M., Bassett, K., Del Carlo, P., Field, B., Frank, T., Hoffmann, S., Kuhn, G., Reichelt, L., Sandroni, S. and Taviani, M. (2008) Petrologic and geochemical composition of the AND-2A core, ANDRILL Southern McMurdo Sound Project, Antarctica. *Terra Antartica*, 15(1), 147-192.

Passchier, S., Browne, G., Field, B., Fielding, C.R., Krissek, L.A., Panter, K., Pekar, S.F., and ANDRILL-SMS Science Team (2011) Early and middle Miocene Antarctic glacial history from the sedimentary facies distribution in the AND-2A drill hole, Ross Sea, Antarctica. *Geological Society of America Bulletin*, 123(11-12), 2352-2365, Available at: doi: 10.1130/B30334.1.

Passchier, S., Falk., C. and Florindo, F. (2013) Orbitally-paced shifts in the particle size of the Antarctic continental shelf in response to ice dynamics during the Miocene Climatic Optimum. *Geosphere*, 9, 54-62, Available at: doi:10.1130/GES00840.1.

Patterson, M. O., McKay, R., Naish, T., Escutia, C., Jimenez-Espejo, F. J., Raymo, M. E., Meyers, S. R., Tauxe, L., Brinkhuis, H., Klaus, A., Fehr, A., Bendle, J. A. P., Bijl, P. K., Bohaty, S. M., Carr, S. A., Dunbar, R. B., Flores, J. A., Gonzalez, J. J., Hayden, T. G., Iwai, M., Katsuki, K., Kong, G. S., Nakai, M., Olney, M. P., Passchier, S., Pekar, S. F., Pross, J., Riesselman, C. R., Röhl, U., Sakai, T., Shrivastava, P. K., Stickley, C. E., Sugasaki, S., Tuo, S., van de Flierdt, T., Welsh, K., Williams, T., and Yamane, M. (2014) Orbital forcing of the East Antarctic ice sheet during the Pliocene and Early Pleistocene. *Nature Geoscience*, 7(11), 841-847.

Powell, R. and Domack, G. (2002) Modern glaciomarine environments, *in* Menzies, J., ed., Past and Modern Glacial Environments. Butterworth-Heinemann, p. 361-389.

Prins, M. A., Bouwer, L. M., Beets, C. J., Troelstra, S. R., Weltje, G. J., Kruk, R. W., Kuijpers, A., and Vroon, P. Z. (2002) Ocean circulation and iceberg discharge in the glacial North Atlantic: Inferences from unmixing of sediment size distributions. *Geology*, 30(6), 555-558. Available at: doi:10.1130/0091-7613(2002)030<0555:OCAIDI>2.0.CO;2.

Ragueneau, O., Savoye, N., Del Amo, Y., Cotten, J., Tardiveau, B., Leynaert, A. (2005) A new method for the measurement of biogenic silica in suspended matter of coastal waters: using Si:Al ratios to correct for the mineral interference. *Continental Shelf Research*, 25, 697–710.

Rosenberg, J. (2014) Late Pliocene ice-rafted debris mass accumulation rates from IODP site U1359, Wilkes Land Continental Rise, Antarctica. M.S. Thesis, Montclair State University, Dept. of Earth and Environmental Studies.

Scherer, R. P., DeConto, R. M., Pollard, D., and Alley, R. B. (2016) Windblown Pliocene diatoms and East Antarctic Ice Sheet retreat. *Nature Communications*, 7, 12957.

Shrivastava, P. K., Dharwadkar, A., Asthana, R., Roy, S. K., Swain, A. K., and Beg, M. J. (2014) The sediment properties of glacial diamicts from the Jutulsessen area of Gjelsvikfjella, East Antarctica: A reflection of source materials and regional climate. *Polar Science*, 8(3), 264-282.

Sperazza, M., Moore, J. N., and Hendrix, M. S. (2004) High-resolution particle size analysis of naturally occurring very fine-grained sediment through laser diffractometry. *Journal of Sedimentary Research*, 74(5), 736-743.

St John, K., Passchier, S., Tantillo, B., Darby, D., And Kearns, L. (2015) Microfeatures of modern sea-ice-rafted sediment and implications for paleo-sea-ice reconstructions. *Annals of Glaciology*, 56(69.

Sweet, D. E., and Brannan, D. K. (2016) Proportion of glacially to fluvially induced quartz grain microtextures along the Chitina River, SE Alaska, U.S.A. *Journal of Sedimentary Research*, 86(7), 749-761.

Taylor-Silva, B. I., and Riesselman, C. R. (2018) Polar frontal migration in the warm late Pliocene: diatom evidence from the Wilkes Land Margin, East Antarctica. *Paleoceanography and Paleoclimatology*, 33(1), 76-92.

Tauxe, L., C.E. Stickley, S. Sugisaki, P.K. Bijl, S.M. Bohaty, H. Brinkhuis, C. Escutia, J.A. Flores, A.J.P. Houben, M. Iwai, F. Jiménez-Espejo, R. McKay, S. Passchier, J. Pross, C.R. Riesselman, U. Röhl, F. Sangiorgi, K. Welsh, A. Klaus, A. Fehr, J.A.P. Bendle, R. Dunbar, J. González, T. Hayden, K. Katsuki, M.P. Olney, S.F. Pekar, P.K. Shrivastava, T. van de Flierdt, T. Williams, and M. Yamane (2012) Chronostratigraphic framework for the IODP Expedition 318 cores from the Wilkes Land Margin: constraints for paleoceanographic reconstruction. *Paleoceanography*, 27(2).

Vos, K., Vandenberghe, N., and Elsen, J. (2014) Surface textural analysis of quartz grains by scanning electron microscopy (SEM): From sample preparation to environmental interpretation. *Earth-Science Reviews*, 128, p. 93-104.

Wellendorf, W., and Krinsley, D. (1980) The relation between the crystallography of quartz, and upturned aeolian cleavage plates. *Sedimentology*, 27, 447-453.

Wentworth, C. K. (1922) A scale of grade and class terms for clastic sediments. *The Journal of Geology*, 30(5), 377-392.

Westerhold, T., Marwan, N., Drury, A. J., Liebrand, D., Agnini, C., Anagnostou, E., Barnet, J. S. K., Bohaty, S. M., De Vleeschouwer, D., Florindo, F., Frederichs, T., Hodell, D. A., Holbourn, A. E., Kroon, D., Lauretano, V., Littler, K., Lourens, L. J., Lyle, M., Pälike, H., Röhl, U., Tian, J., Wilkens, R. H., Wilson, P. A., and Zachos, J. C. (2020) An astronomically dated record of Earth's climate and its predictability over the last 66 million years. *Science*, 369(6509), 1383-1387.

Whalley, W. B., and Langway, C.C. (1980) A scanning electron microscope examination of subglacial quartz grains from Camp Century core, Greenland-a preliminary study. *Journal of Glaciology*, 25(91), 125-131.

Whalley, W. B., and Krinsley, D. H. (1974) A scanning electron microscope study of surface textures of quartz grains from glacial environments. *Sedimentology*, 21(1), 87-105.

Whitehead, J. M., Wotherspoon, S., and Bohaty, S. M. (2005) Minimal Antarctic sea ice during the Pliocene. *Geology*, 33(2), 137.

Woronko, B., and Hoch, M. (2011) The development of frost-weathering microstructures on sand-sized quartz grains: examples from Poland and Mongolia. *Permafrost and Periglacial Processes*, 22(3), 214-227.

Woronko, B., and Pisarska-Jamroży, M. (2016) Micro-Scale frost weathering of sand-sized quartz grains. *Permafrost and Periglacial Processes*, 27, 109– 122, Available at: doi: 10.1002/ppp.1855.

FIGURE CAPTIONS

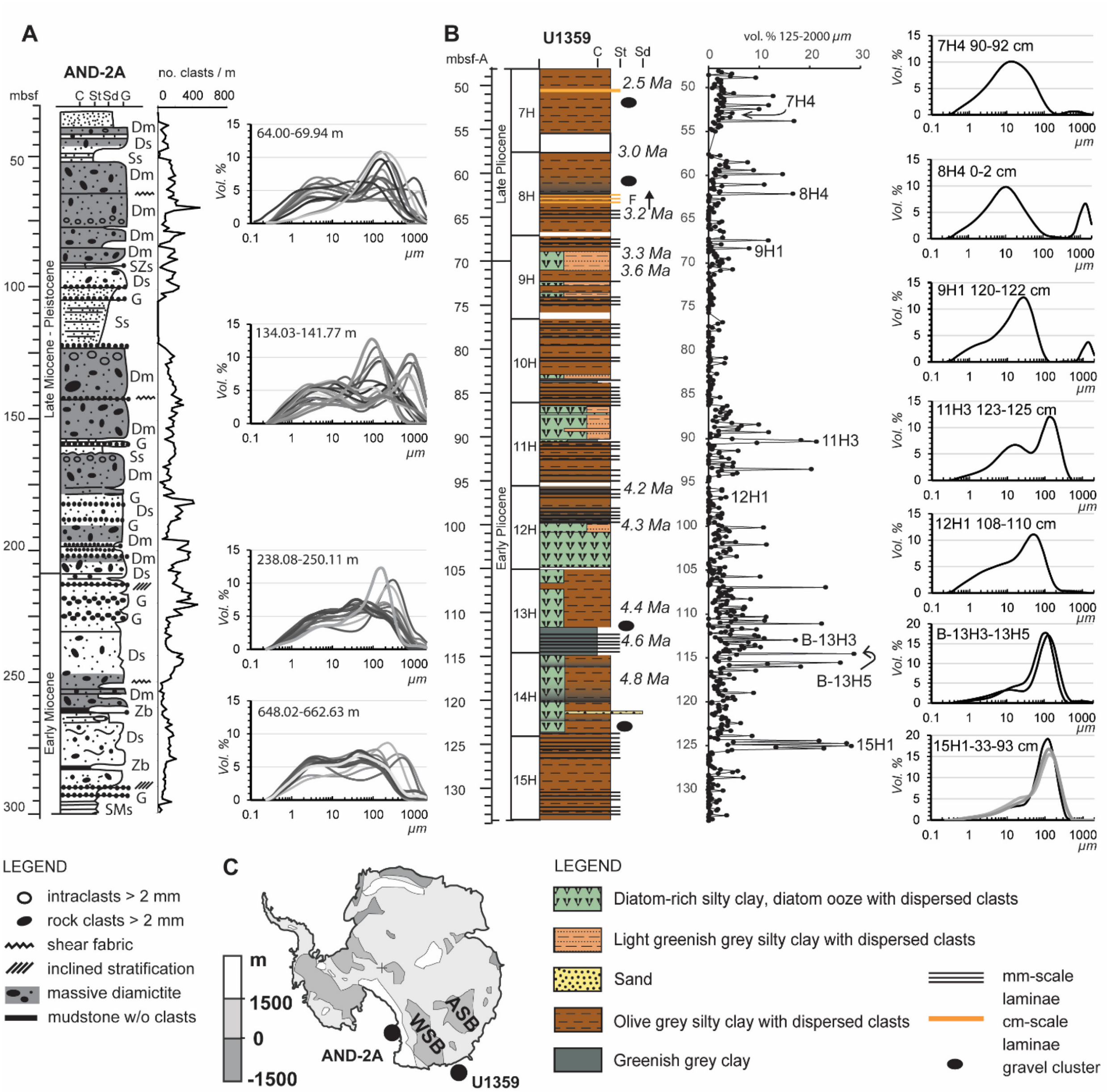

Figure 1. Lithological column and terrigenous particle-size distributions for SEM samples in the upper *ca* 300 m of the ANDRILL Site 2A (AND-2A) drillcore (A) and Integrated Ocean Drilling Program (IODP) Site U1359 (B). Dm: Massive diamictite; Ds: Stratified diamictite; G: Gravel; Ss: Sandstone; SZs: Sandy siltstone; SMs: Sandy mudstone; Zb: Clayey siltstone. Locations of drill sites are indicated in panel (C). WSB: Wilkes Subglacial Basin; ASB: Aurora Subglacial

Basin. Particle-size distributions of all 46 samples are shown in (A), whereas only the particle-size distributions for samples investigated via SEM are shown in (B).

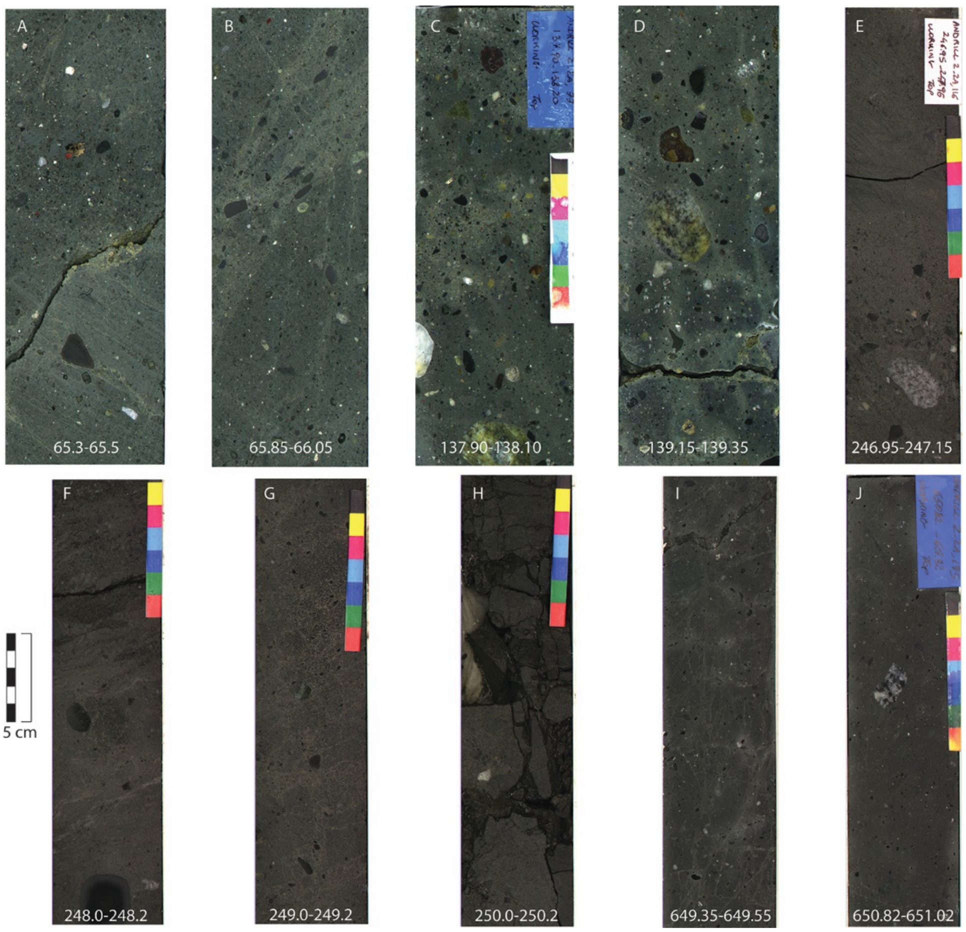

Figure 2. Core images of AND-2A drillcore sections sampled for both SEM and particle-size analysis. Depth range is in metres below seafloor (mbsf). Samples originate from the center of each of the intervals. Sample depth below seafloor and lithology is listed in Table 1.

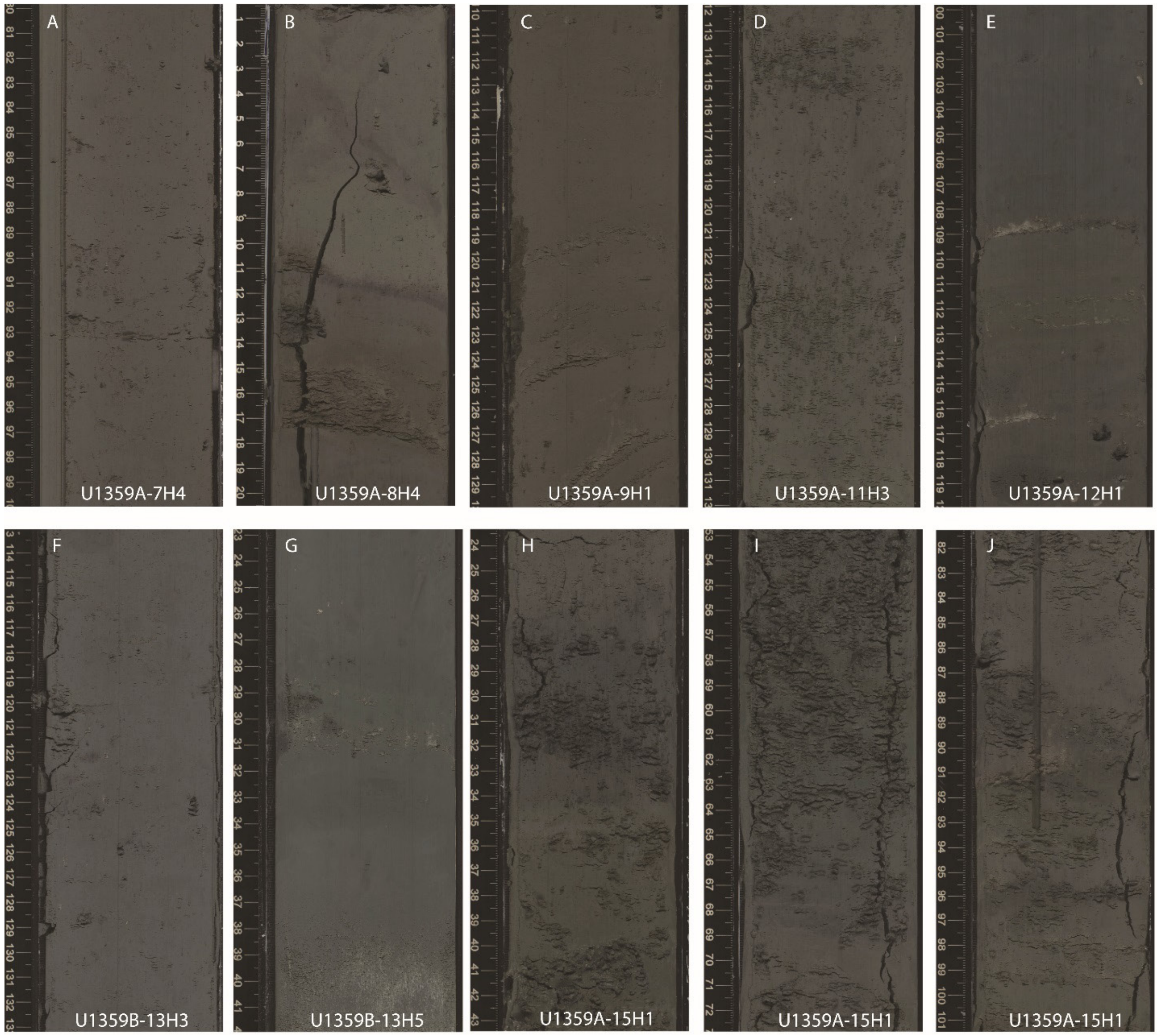

Figure 3. Core images of IODP Site U1359 drillcore sections sampled for SEM and particle-size analysis. Samples originate from the center of each of the intervals. Sample depth below seafloor and lithology is listed in Table 1.

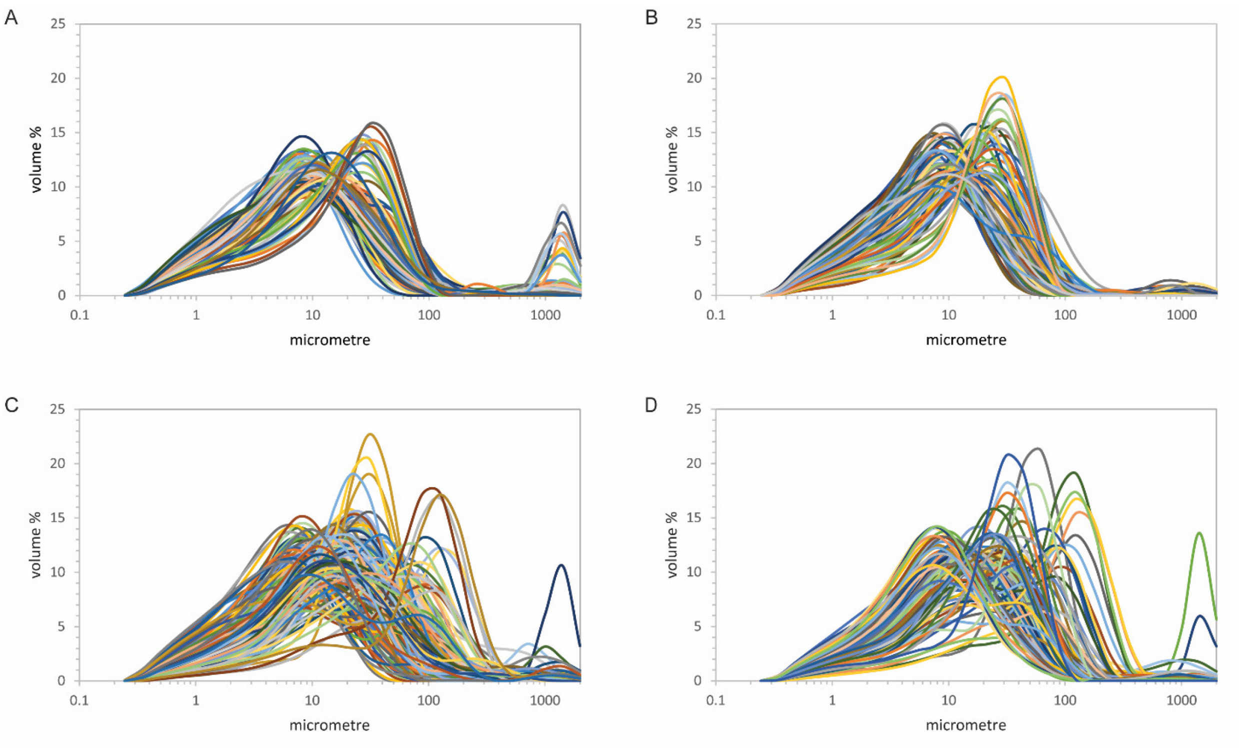

Figure 4. Grain-size distributions for samples from IODP Site U1359. (A) Upper Pliocene silty clay with dispersed sand and gravel in core interval U1359A-7H1, to -9H2 dated *ca* 3.3-2.7 Ma; (B) Lower Pliocene diatom-bearing silty clay with dispersed sand and gravel in core interval U1359A-9H2 to -11H1 dated *ca* 4.0-3.3 Ma; (C) Lower Pliocene diatom-rich silty clay and ooze with dispersed sand and gravel in core interval U1359A-11H1 to U1359B-13H5 dated *ca* 4.7-4.0 Ma; (D) Lower Pliocene diatom-bearing silty clay with dispersed sand and gravel in core interval U1359A-14H1 to -15H-7. The lithological log, core labels and age tie points are shown in Figure 1 and macroscopic characteristics of facies are depicted in Figure 3.

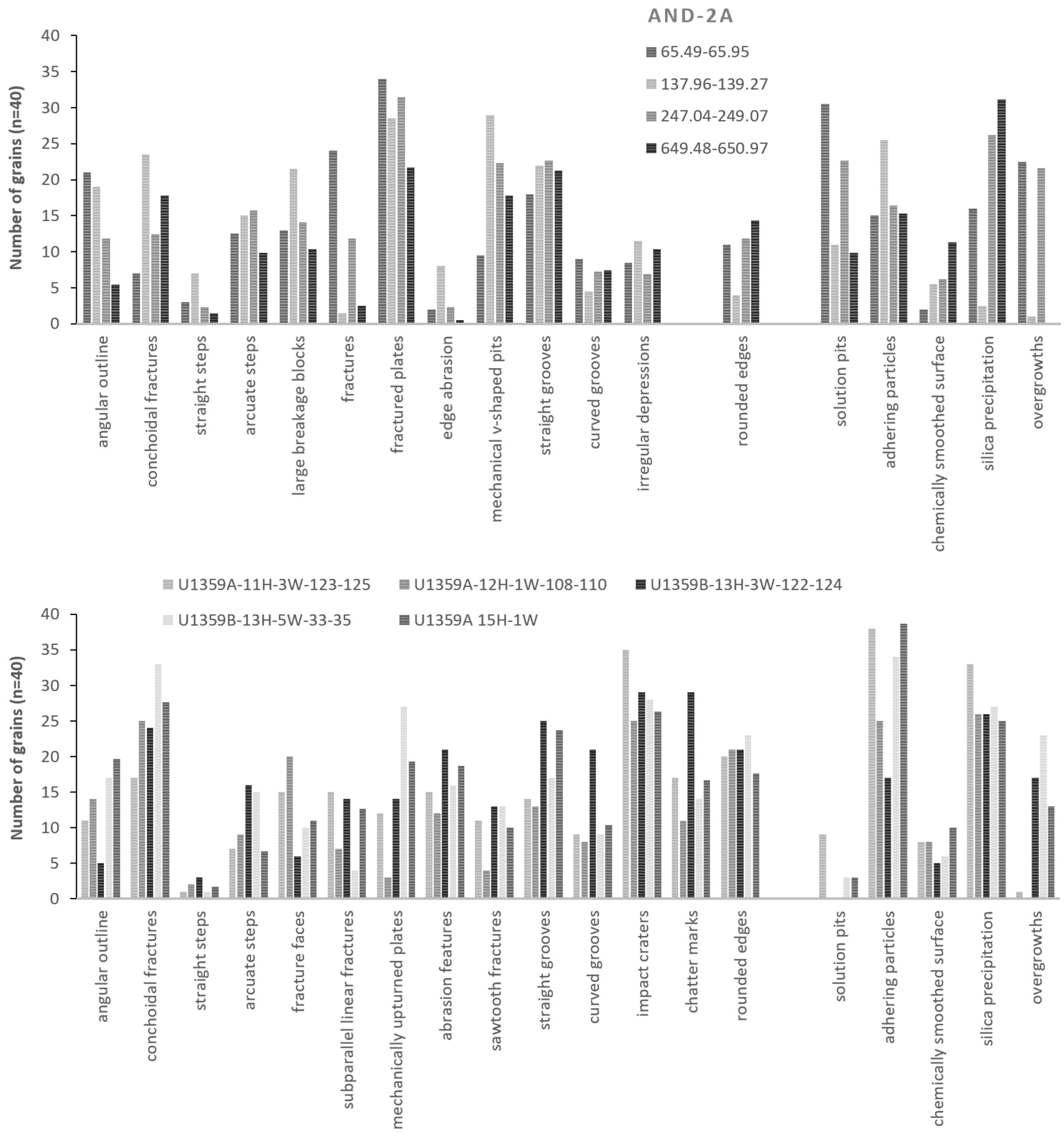

Figure 5. Frequency distributions of individual microtextures in samples from (A) AND-2A and (B) IODP Site U1359.

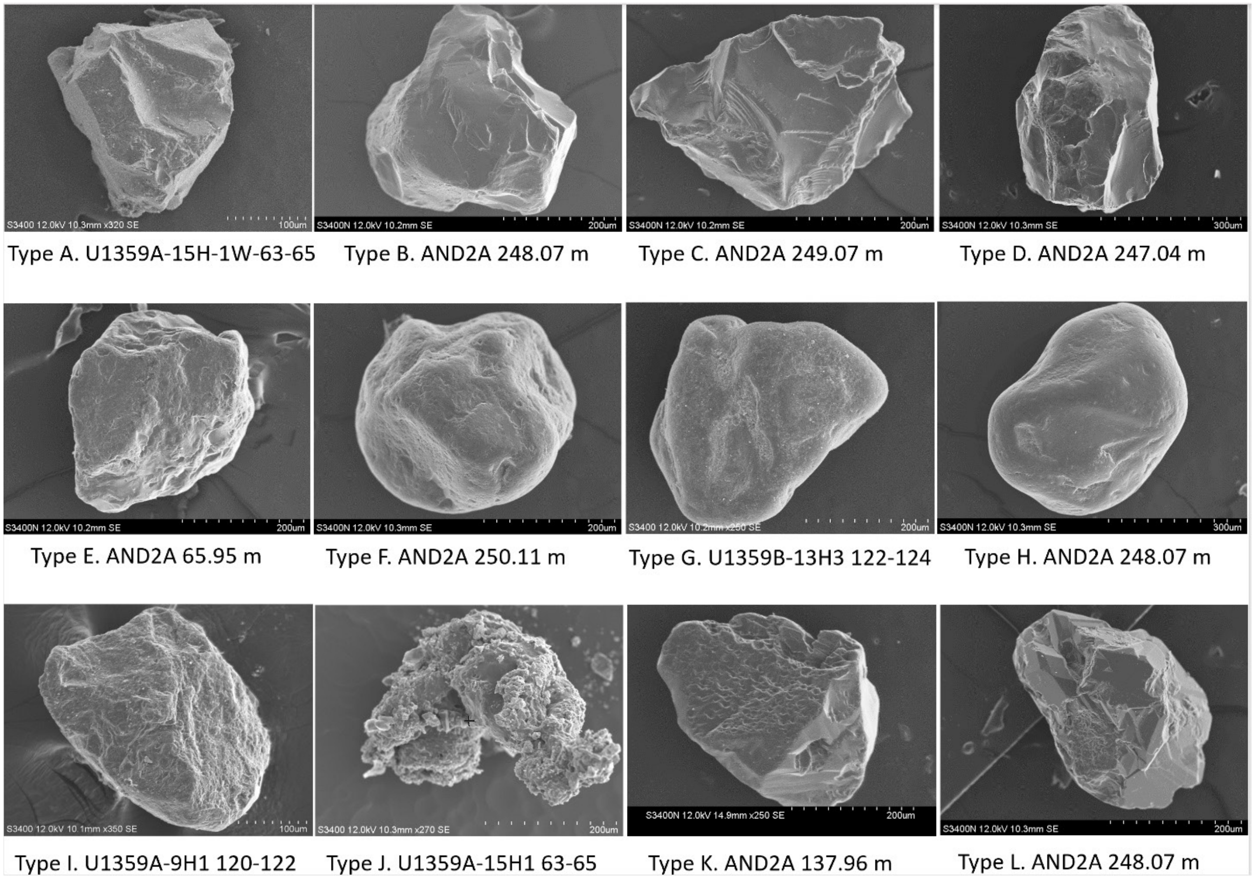

Figure 6. Secondary Electron images of grain types characterised in sand fractions from diamicts sampled in ANDRILL Site 2A (AND-2A) and ice-rafted debris from Integrated Ocean Drilling Program (IODP) Site U1359.

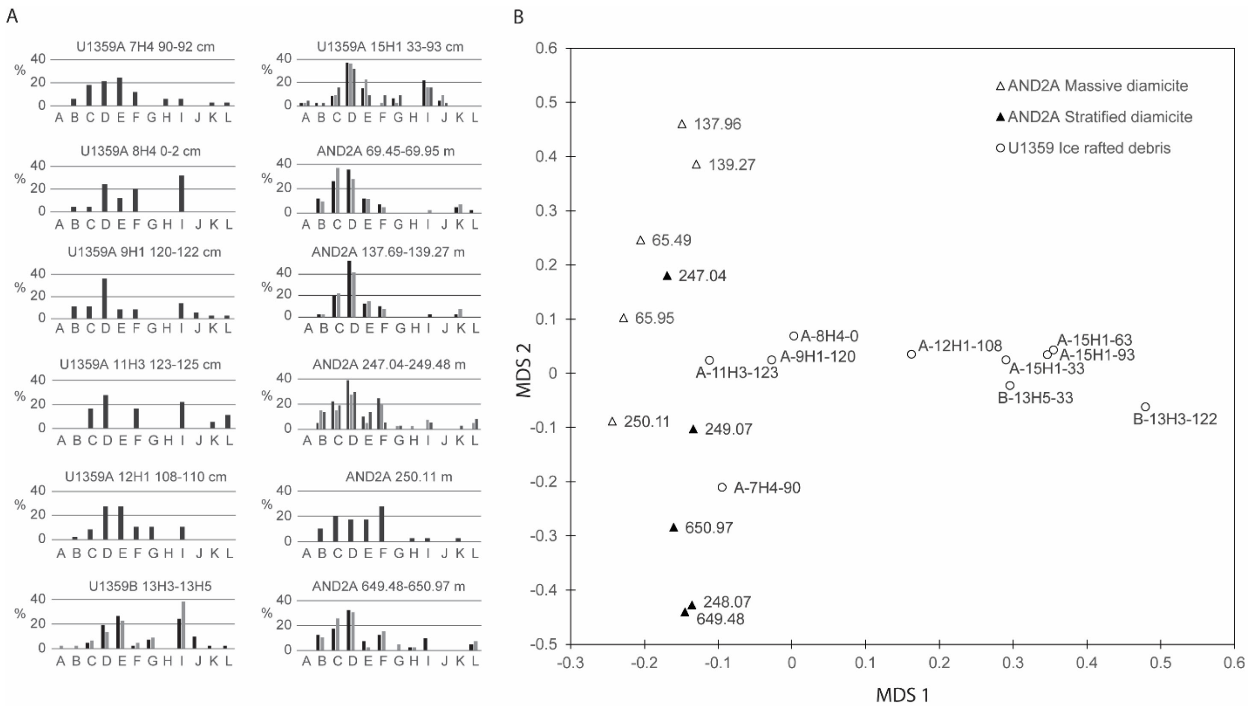

Figure 7. (A) Frequency distributions per sample for grain types A-L depicted in Figure 6, and (B) plot of metric multidimensional scaling for the 20 individual samples.

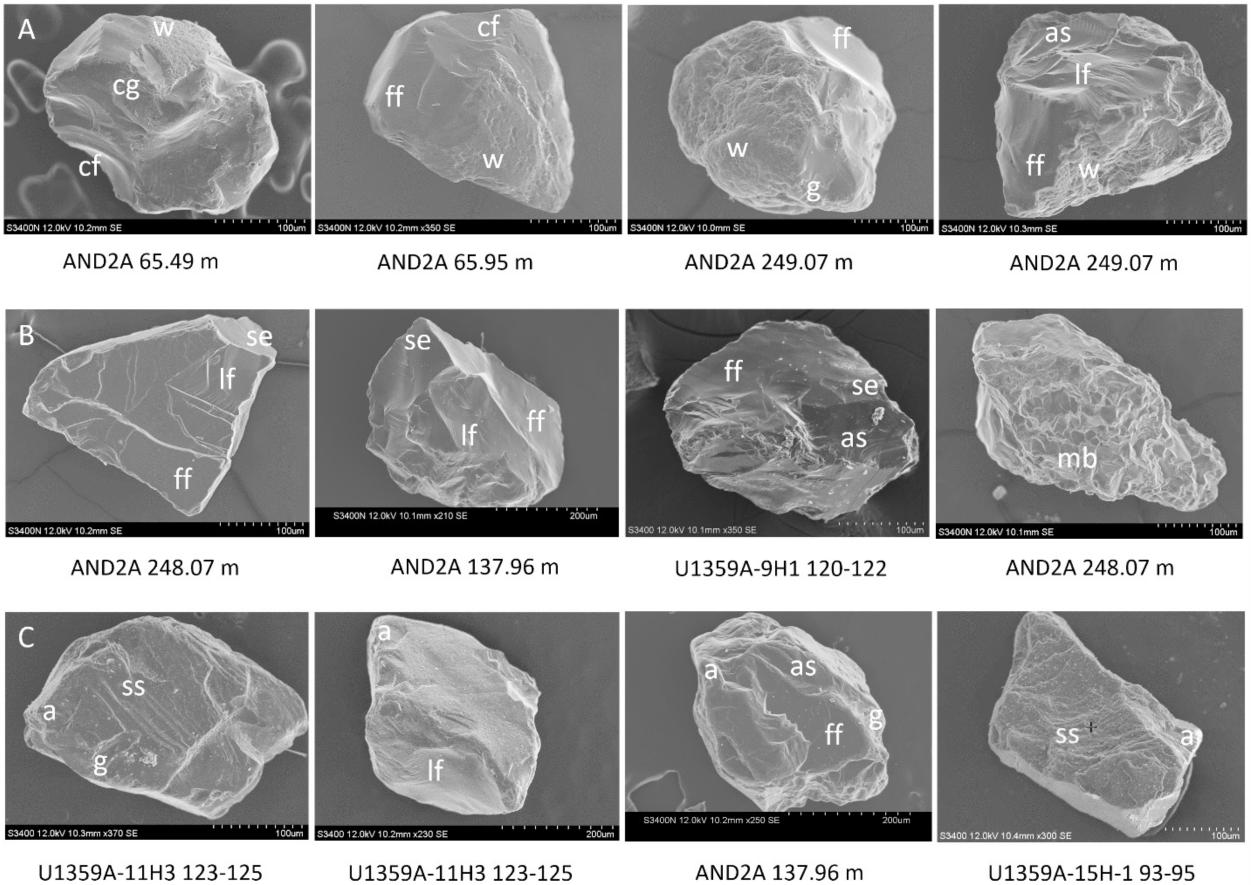

Figure 8. Panel (A) shows Type B grains, panel (B) shows Type C grains, and panel (C) Type D grains. Microtexture codes are indicated as follows: w = pre-weathered surface; cg = crescentic gouge; cf = conchoidal fracture; ff = fracture faces; lf = linear fractures; se = sharp edges; ss = straight steps; g = grooves; a = edge abrasion; as = arcuate steps; mb = microblocks.

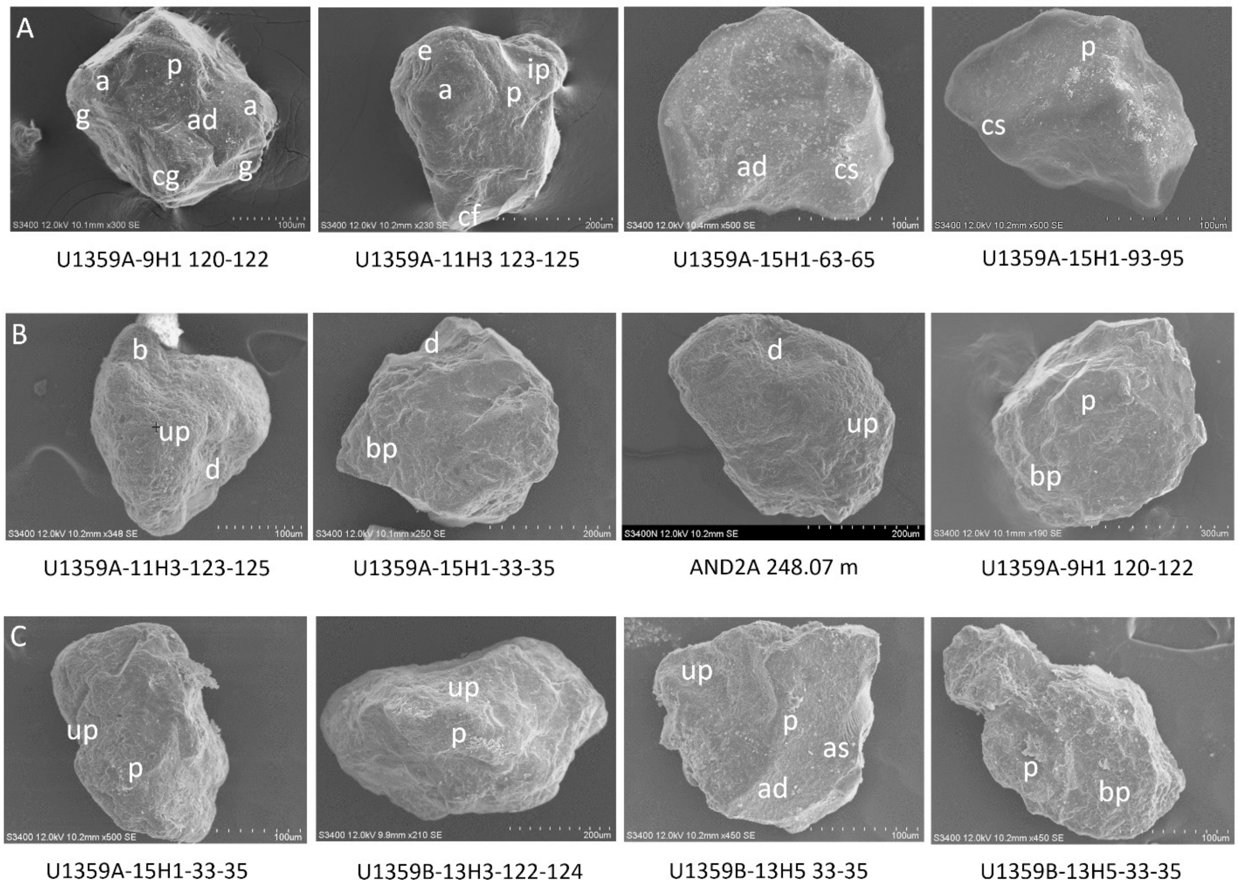

Figure 9. Panel (A) shows Type E grains, and (B) and (C) show Type I grains. Microtexture codes are indicated as follows: a = edge abrasion; p = silica precipitation; cg = crescentic gouge; g = groove; ad = adhering particles; ip = impact mark; e = etching; cf = conchoidal fracture; cs = chemical smoothing; up = upturned plates; bp = broken plates; b = bulbous edge; d = dish-shaped depression; as = arcuate steps

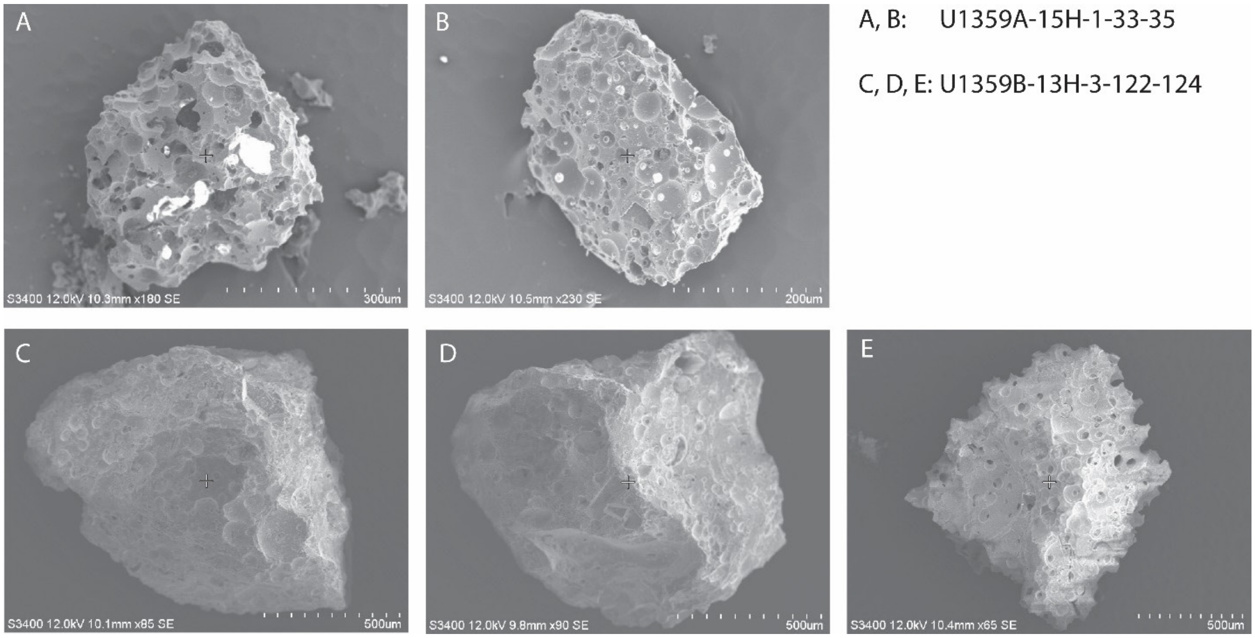

Figure 10. Abraded vesicular basalt grains in samples from the lower Pliocene interval at Site U1359.

TABLE 1. List of Scanning Electron Microscopy samples selected from the AND-2A drillsite in the Ross Sea, and the U1359 drillsite on the Wilkes Land continental margin, Antarctica

Sample ID	mbsf	Lithology
AND2A 65.49	65.49	clast-poor sandy diamictite, possible shear structure
AND2A 65.95	65.95	clast-rich sandy diamictite, possible shear structure
AND2A 137.96	137.96	massive clast-rich sandy diamictite
AND2A 139.27	139.27	massive clast-rich sandy diamictite with brecciated fabric
AND2A 247.04	247.04	volcanic-bearing clast-rich sandy diamictite, possible shear structure
AND2A 248.07	248.07	volcanic-bearing clast-rich sandy diamictite, possible shear structure
AND2A 249.07	249.07	volcanic-bearing clast-rich sandy diamictite, possible shear structure
AND2A 250.11	250.11	volcanic-bearing clast-rich sandy diamictite, brecciated fabric
AND2A 649.48	649.48	volcanic-bearing clast-poor muddy diamictite
AND2A 650.97	650.97	volcanic-bearing clast-poor muddy diamictite
U1359A-7H-4W-90-92	53.5	silty clay with dispersed clasts
U1359A-8H-4W-0-2	62.1	silty clay with dispersed clasts (above normally graded laminae)
U1359A-9H-1W-120-122	68.3	laminated silty clay with dispersed clasts
U1359A-11H-3W-123-125	90.33	diatom-rich silty clay with dispersed clasts
U1359A-12H-1W-108-110	96.68	laminated silty clay with dispersed clasts
U1359B-13H-3W-122-124	113.42	diatom-rich clay with dispersed clasts, sand pockets
U1359B-13H-5W-33-35	118.53	diatom-rich clay with dispersed clasts, sand pockets
U1359A-15H-1W-33-35	124.43	silty clay with dispersed clasts
U1359A-15H-1W-63-65	124.73	silty clay with dispersed clasts
U1359A-15H-1W-93-95	125.03	laminated silty clay with dispersed clasts w/ normally graded sand/silt

TABLE 2. Description and interpretation of grain types

Type	Roundness	Relief	Textures	Interpretation
A	very angular to angular	medium	fractures	in situ physical weathering, immature sediment
B	subangular to subrounded	medium	altered/rounded surfaces overprinted by steps, parallel fractures, conchoidal fractures	glacial plucking, crushing and/or abrasion of pre-existing sediments
C	very angular to subangular	high	steps, parallel fractures, conchoidal fractures, microblocks	glacial plucking, crushing and/or abrasion
D	subangular to subrounded	high	steps, parallel fractures, conchoidal fractures, microblocks, edge rounding	glacial plucking, crushing and/or abrasion followed by current transport
E	subangular to subrounded	high	smoothed/abraded fracture surfaces, edge rounding, precipitation	glaciofluvial or littoral sediment
F	subrounded	medium	v-shaped percussion marks, conchoidal fractures, grain breakage	subaqueous current transport
G	subangular to subrounded	medium	edge rounding, dissolution	chemical weathering of flood plain sediment
H	rounded to well-rounded	low	v-shaped percussion marks, solution pits	eolian transport and chemical weathering
I	subangular to subrounded	high to medium	polygenetic upturned plates, precipitation, dish-shaped depressions	eolian transport and chemical weathering
J	angular to subangular	high to medium	adhering particles, precipitation	physical and chemical weathering of immature sediment
K	subangular to subrounded	high to medium	strong solution exposing lattice, crystalline etch pits	strong chemical alteration of sediment
L	subrounded	medium	solution and euhedral crystalline overgrowth	strong chemical alteration of sediment